Discover Oncology

Research

Tanshinone IIA affects the proliferation of A549/Tax by affecting the expression of MMP7 through the PI3K-AKT-mTOR signaling pathway

Fangjun Chen[1,2] · **Wenqiong Xiang**[3] · **Guangliang Qiang**[4]

Received: 10 December 2024 / Accepted: 14 March 2025
Published online: 20 March 2025

Abstract

Objective This study aims to explore whether tanshinone IIA can act on paclitaxel-resistant non-small cell lung cancer A549/Tax and analyze the possible mechanisms involved.

Methods Using the Cell Counting Kit-8 (CCK-8), we preliminarily analyzed whether tanshinone IIA has an inhibitory effect on A549/Tax cells. We utilized public datasets, self-collected transcriptome datasets, and drug target analysis to identify potential targets. We employed real-time fluorescent quantitative polymerase chain reaction (RT-qPCR) to detect the expression of core genes before and after drug treatment to analyze potential target genes and validated them using data from The Cancer Genome Atlas (TCGA). We conducted enrichment analysis on co-expressed genes of the target genes to explore potential mechanisms. Furthermore, we employed molecular docking and western blot to verify the possible mechanisms involved.

Results The CCK8 results indicated that tanshinone IIA has a significant inhibitory effect on A549/Tax cells. The qPCR results and the analysis of TCGA data indicated that MMP7 is the target gene. Enrichment results of MMP7 co-expressed genes suggested that the PI3K-AKT signaling pathway might play a key role. Molecular docking results indicated that tanshinone IIA has strong binding activity with PI3K, AKT, mTOR, and MMP7. Western blotting results showed that tanshinone IIA might inhibit MMP7 through the PI3K-AKT-mTOR signaling pathway.

Conclusions Tanshinone IIA may affect the proliferation of A549/Tax by influencing the expression of MMP7 through the PI3K-AKT-mTOR signaling pathway.

Keywords Lung cancer · Tanshinone IIA · PI3K-AKT signaling pathway · Proliferation · Drug resistance

Supplementary Information The online version contains supplementary material available at https://doi.org/10.1007/s12672-025-02152-8.

✉ Guangliang Qiang, pkudd@bjmu.edu.cn | [1]Department of Thoracic Surgery, China Japan Friendship Institute of Clinical Medicine Research, Beijing, China. [2]Department of Thoracic Surgery, China-Japan Friendship Hospital, Beijing, China. [3]Department of Hematology, The First Affiliated Hospital of Chongqing Medical University, Chongqing, China. [4]Department of Thoracic Surgery, Peking University Third Hospital, No.49 Huayuan North Road, Haidian District, Beijing 100191, China.

1 Introduction

Globally, the number of newly diagnosed lung cancer cases in 2022 reached 2.4803 million, topping the list of all cancers, with lung cancer-related deaths accounting for the majority of all cancer-related deaths and claiming over 1.8 million lives annually [1–3]. According to histological classification, lung cancer is divided into small cell lung cancer and non-small cell lung cancer (NSCLC), with approximately 80–85% of patients diagnosed with NSCLC upon pathological examination [4–6]. Surgical tumor resection has always been the preferred option for early-stage NSCLC patients, provided that the tumor is resectable and the patient can tolerate the surgery [7]. However, due to the unobtrusive and nonspecific early symptoms of lung cancer, the detection rate at an early stage is low, leading to many patients being diagnosed at an advanced stage with poor prognosis and high mortality [8]. Moreover, due to the presence of distant metastasis, most advanced-stage patients lose the opportunity for surgery, and medical treatment becomes their preferred treatment option. Despite promising therapeutic methods including immunotherapy, chemotherapy, radiotherapy, and surgery, the overall survival rate remains poor [9–12]. Therefore, it is particularly important to seek new therapeutic drugs for lung cancer patients.

Paclitaxel is a well-known chemotherapeutic drug used to treat various cancers, including lung cancer [13]. However, patients with NSCLC are prone to develop resistance to first-line paclitaxel chemotherapy [14]. Despite some progress in recent years, challenges still exist in identifying predictive biomarkers for personalized treatment and overcoming resistance [15]. It is important to seek follow-up treatments for patients with paclitaxel-resistant lung cancer or to overcome drug resistance.

Tanshinone IIA is an active component extracted from the plant Salvia miltiorrhiza, and its dry roots form the traditional Chinese medicine Danshen. Numerous previous studies have shown that tanshinone IIA can be used to inhibit the growth of lung cancer cells [16–18]. Additionally, several studies have indicated that tanshinone IIA can overcome lung cancer resistance, including resistance to osimertinib and gefitinib [19–21], and further studies have shown that tanshinone IIA can enhance the efficacy of anti-PD-1 immunotherapy, cisplatin, and doxorubicin treatments [22–24]. However, no studies have yet demonstrated its effectiveness against paclitaxel-resistant NSCLC.

Therefore, this study aims to explore whether tanshinone IIA can help inhibit the growth of paclitaxel-resistant NSCLC and whether tanshinone IIA can restore the sensitivity of paclitaxel-resistant NSCLC to paclitaxel, as well as to analyze the possible mechanisms involved.

2 Methods

This study did not involve patient information or animal experiments, so we did not apply for any specific ethical consent. This study was conducted in accordance with the Declaration of Helsinki.

2.1 Cell culture

Human normal lung epithelial cell line BEAS-2B and paclitaxel-resistant non-small cell lung cancer cell line A549/Tax were purchased from the Shanghai Cell Bank of the Chinese Academy of Sciences. The human non-small cell lung cancer cell line A549 was received from Dr. Jiao Qiao at Peking University Third Hospital. BEAS-2B and A549 were cultured in RPMI-1640 medium (PM150110, Procell) containing 10% fetal bovine serum (164,210, Procell) and 1% streptomycin (P1400-100 m, Solarbio). A549/Tax was cultured in A549/Tax complete medium (CM-0585, Procell). Cells were incubated in a humidified incubator at 37 °C with 5% CO2.

2.2 Cell viability assay

Cell viability was assessed using the CCK-8 (C0039, Beyotime) according to the manufacturer's instructions. In brief, 5 × 10^3 cells were seeded in 100 µl of medium in a 96-well plate and then treated with varying concentrations of paclitaxel (FK20456-5 mg, FreeMoreBio) for A549 (10–80 ng/ml) and A549/Tax (6–20 µg/ml) to verify the authenticity of the cell lines. To analyze the effectiveness of tanshinone IIA, different concentrations were used for A549 (5–40 µmol/L) and

A549/Tax (10–80 µmol/L), and to assess drug safety, BEAS-2B cells was treated (50–100 µmol/L) for 24 h. After treatment, 10 µl of CCK-8 solution was added to each well, and the cells were further incubated for 1 h at 37 °C and 5% CO2. The absorbance was measured at 450 nm using a SYNERGY absorbance reader (BioTek Instruments, Inc.).

2.3 Core gene analysis

Initially, the dataset GSE243455 from the Gene Expression Omnibus (GEO) database was analyzed with a screening threshold of $p < 0.05$ and $|\log2(\text{fold change})| \geq 1$ to identify differentially expressed genes between A549 and BEAS-2B. Subsequently, our self-collected dataset obtained from BGI (Shenzhen) was analyzed with a screening threshold of $p < 0.01$ and $|\log2(\text{fold change})| \geq 2$ to identify differentially expressed genes between A549/Tax and A549. The intersection of these genes was used to identify genes that were sequentially upregulated/downregulated in BEAS-2B, A549, and A549/Tax. The potential targets of tanshinone IIA obtained from the SwissTargetPrediction (http://www.swisstargetprediction.ch/) and GeneCards (https://www.genecards.org/) databases were merged and intersected with the gradient differentially expressed genes to predict key targets of tanshinone IIA that may play a role in inhibiting A549 and potentially A549/Tax. These targets were imported into the STRING database (https://string-db.org/), with "Homo sapiens" set as the protein species, hiding isolated nodes, to construct a protein–protein interaction (PPI) network. The results were saved in tsv format and imported into Cytoscape 3.9.0 software, where the cytoHubba plugin's Maximum Clique Centrality (MCC) algorithm was used to screen for core gene modules from the PPI network.

2.4 qPCR and validation

Total RNA was extracted from cells using the SteadyPure Quick RNA Extraction Kit (AG2102) according to the manufacturer's instructions (Accurate biotechnology). RNA was reverse-transcribed into cDNA using the Evo M-MLV RT Mix Kit with gDNA Clean for qPCR Ver.2 (AG1172). Quantitative PCR analysis was performed using the SYBR Green Premix Pro TaqHS qPCR Kit (Low Rox Plus) (AG11739) on the QuantStudio 5 (Thermo Fisher Scientific, USA). Primers were as follows:

Human CCL2: 5′-CTTCTGTGCCTGCTGCTCATA-3′(primer F), 5′-CTTTGGGACACTTGCTGCTG-3′(primer R);
Human CTSS: 5′-TGCGCGTCATCCTTCTTTCT-3′(primer F), 5′-AGCCAACCACAAGTACACCA-3′(primer R);
Human MMP2: 5′-CTCATCGCAGATGCCTGGAA-3′(primer F), 5′-TTCAGGTAATAGGCACCCTTGAAGA-3′(primer R);
Human MMP7: 5′-CTCGGAGGAGATGCTCACTTC-3′(primer F), 5′-AGGAATGTCCCATACCCAAAGAAT-3′(primer R);
Human β-actin: 5′-TGGCACCCAGCACAATGAA-3′(primer F), 5′-CTAAGTCATAGTCCGCCTAGAAGCA-3′(primer R).

qPCR conditions were as follows: pre-denaturation at 95 °C for 30 s, followed by denaturation at 95 °C for 5 s and annealing/extension at 60 °C for 30 s, for a total of 40 cycles. The relative expression levels of all genes were calculated using the $2^{-\Delta\Delta Ct}$ formula. We further downloaded, organized, and analyzed the relative expression of the aforementioned core genes in lung cancer and normal controls from the TCGA database (https://portal.gdc.cancer.gov) as a validation set for the qPCR results.

2.5 Enrichment analysis

We utilized the online tool GeneMANIA (http://genemania.org/) to exploring gene interactions and functions, as well as identifying co-expressed genes [25]. The clusterProfiler (4.2.2) package in R was used for gene ontology (GO) and Kyoto Encyclopedia of Genes and Genomes (KEGG) pathway analysis of the co-expressed genes, where GO enrichment analysis included Molecular Function (MF), Biological Process (BP), and Cellular Component (CC), with a significance threshold set at $p < 0.05$.

2.6 Diagnostic and prognostic value of core genes for lung adenocarcinoma and squamous cell carcinoma

We extracted the RNAseq data in TPM format for lung adenocarcinoma and squamous cell carcinoma corresponding to the TCGA data processed by the Toil pipeline and the normal tissue data from GTEx at UCSC XENA (https://xenabrowser.net/datapages/) [26]. The pROC package (1.18.0) in R (4.2.1) was used for receiver operating characteristic (ROC) analysis of the data, with results visualized using ggplot2 (3.3.6). We downloaded and organized the RNAseq data in TPM format and clinical data from the TCGA-LUAD and TCGA-LUSC projects processed by the STAR pipeline from the TCGA database (https://portal.gdc.cancer.gov/), and extracted the TPM format data. Prognosis data were obtained from previous studies [27], and after removing normal and data without clinical information, the surv_cutpoint function in

the survminer package (0.4.9) was used for optimal grouping cut-off selection, and the survival package (3.3.1) was used for proportional hazards assumption testing and fitting survival regression, with results visualized using the survminer package and ggplot2 package.

2.7 Molecular docking

The protein was downloaded from the PDB database, water molecules and receptor proteins were removed using PyMOL software [28], and saved in PDB format, then imported into the AutoDockTools software [29], followed by hydrogenation, calculation of charge, setting of atomic type, and output to the software's special format upon completion. ChemDraw was used to draw the molecular structure of small molecules, and then the small molecules were imported into ChemDraw 3D software to optimize the small molecule structure, with output completed in PDB format. The AutoDockTools software was used to open the small molecule file, perform hydrogenation, calculate the maximum number of rotatable bonds, and set the keys that can be rotated. After setting as a ligand, it was exported to a dedicated format.

The active ingredient structure was docked with the target molecule using the PyRx software (https://pyrx.sourceforge.io/) internal vina for docking. The Affinity (kcal/mol) value represents the binding capacity of the two, with a lower binding capacity indicating a more stable bond between the ligand and the receptor. It is generally believed that a docking energy value less than − 4.25 kcal/mol indicates a certain binding activity between the two, less than − 5.0 kcal/mol indicates a good binding activity, and less than − 7.0 kcal/mol indicates a strong binding activity.

Finally, AutoDockTools is used to open and output the results as a PDB format file, and PyMOL is used to open it. The compounds were introduced into PyMOL, and the optimal model was selected from 9 small molecule conformations to analyze the interactions between the compounds and proteins. Proteins are represented as pink stick structures, molecules as blue stick structures, and hydrogen bonds are indicated by yellow dashed lines.

2.8 Molecular dynamics simulation

Protein ligand complexes were prepared by GROMACS 2024–2, ORCA, Multiwfn and sobtop. We utilized GROMACS as the backend engine with a common simulation setting for all complexes, providing a capability of high-throughput MD simulations. Specifically, this pipeline comprises four stages: preparation, minimization, equilibration, and production simulations. In the system preparation stage, a protein topology is generated using pdb2gmx with the amber14sb force field with the tip3p explicit water model; the ligand parameter and topology are generated with SobTop. Then, a cubic simulation box is used with a minimum distance of 1.2 nm between the protein–ligand complex and the box boundaries. Once the simulation box is prepared, an energy minimization process is carried out to remove the atomic clashes and optimize the geometry of all molecules. In the equilibration simulation stage, a thermostat is applied to heat the system from 0 to 300 K within 100 ps. The heated system is then further equilibrated to 1 bar in an NPT ensemble for another 100 ps. During the equilibration stage, the bonds for molecules are constrained. For the final production stage, the leap-frog algorithm [30] is used for integrating Newton's equations of motion and a Particle Mesh Ewald (PME) [31] method is used for calculating long-range electrostatic interactions. The LINCS [32] algorithm is adopted for reset all bonds to their correct lengths after an unconstrained update. After relaxation, the systems were submitted to 30 ns production simulations with an integration time step of 2 fs.

2.9 Western blotting

PI3K activator 740 Y-P and inhibitor BKM120 were purchased from Macklin (Y860417-5 mg) and Beyotime (SF2726-10 mM), respectively. MMP inhibitor marimastat (SD7176-10 mM) was also purchased from Beyotime. RIPA lysis buffer (R0010-100 ml), protease inhibitor (P6730-1 ml), and phosphatase inhibitor (P1260-1 ml) were all purchased from Solarbio. The primary antibodies included PI3K (SC-365404, SANTA CRUZ), p-AKT (WLP001a, Wanleibio), AKT (WL0003b, Wanleibio), BAX (T40051, Abmart), BCL-2 (T40056, Abmart), mTOR (YT2913, Immunoway), MMP7 (67990-1-IG-100UL, Proteintech), and β-ACTIN (3700S, Cell Signaling Technology). Secondary antibodies, including goat anti-rabbit IgG (LF102) and goat anti-mouse IgG (LF10), ECL detection reagent kit (SQ201), PAGE gel rapid preparation kit (PG212), electrophoresis buffer (PS105S), and transfer buffer (PS109S) were all purchased from EpiZyme.

Cells, including untreated BEAS-2B, A549, and A549/Tax, as well as A549/Tax treated with drugs (+Tanshinone IIA, +BKM120, +Tanshinone IIA + 740 Y-P, +Marimastat), were lysed using RIPA lysis buffer containing 1% protease inhibitor and 1% phosphatase inhibitor. The prepared proteins were separated by gel electrophoresis and then transferred onto

membranes. After blocking these membranes with BSA, they were incubated with the primary antibodies overnight at 4 °C. After incubation, the membranes were incubated with the corresponding secondary antibodies for 60 min and the protein bands were visualized using enhanced chemiluminescence in a gel imaging system (Bio-Rad). ImageJ was used to adjust the sample loading and quantify the proteins.

2.10 Statistical analysis

The analysis and visualization of qPCR and western blot results were performed using GraphPad Prism version 9.3.0 (GraphPad Software, LLC). Statistical significance was indicated by $p < 0.05$.

3 Results

3.1 Tanshinone IIA is effective against A549/Tax

To explore and verify the correctness of the cell line and drug and whether tanshinone IIA has an inhibitory effect on A549/Tax while being safe for BEAS-2B, different concentrations of paclitaxel were used on A549(10–80 ng/ml) and A549/Tax(6–20 μg/ml), and different concentrations of tanshinone IIA were used on BEAS-2B(50–100 μmol/L), A549(5–40 μmol/L) and A549/Tax (10–80 μmol/L). The action time was 24 h.

The CCK8 results indicated that the IC50 of paclitaxel for A549 and A549/Tax were 20-30 ng/ml and greater than 20ug/ml, respectively, which is generally consistent with the results of previous studies [33–35], indirectly confirming the correctness of paclitaxel and cell lines. The IC50 of tanshinone IIA for A549 and A549/Tax were 15–20 and 70–80 umol/L, respectively, and the IC50 for BEAS-2B was greater than 100umol/L, demonstrating the safety of tanshinone IIA for normal alveolar epithelial cells. The results of tanshinone IIA on A549 were generally consistent with previous studies [23, 36], indirectly confirming the correctness of tanshinone IIA. The results are shown in Fig. 1a–d. All N = 3.

3.2 MMP7 is the core gene

To analyze genes that play a key role in inhibiting A549/Tax, we analyzed and validated potential core genes using public datasets, transcriptome sequencing data, and qPCR.

The analysis of the dataset GSE243455 revealed that 1553 genes were significantly upregulated and 2180 genes were significantly downregulated in A549 compared to BEAS-2B. Analysis of the transcriptome sequencing data showed that 1294 genes were significantly upregulated and 548 genes were significantly downregulated in A549/Tax compared to A549. Subsequent analysis identified 145 genes that sequentially increased and 71 genes that sequentially decreased across BEAS-2B, A549, and A549/Tax. Additionally, we obtained 258 potential target genes from GeneCards and SwissTarget, and intersected them with the aforementioned 216 (145 + 71) stepwise varying genes, yielding 8 intersecting genes. Subsequently, using the STRING database and Cytoscape 3.9.0 software, we identified 4 potential core genes (CCL2, CTSS, MMP2, MMP7) that sequentially increased in BEAS-2B, A549, and A549/Tax. The results are shown in Fig. 1e–j.

The qPCR results showed that there was no significant difference in MMP2 expression between BEAS-2B and A549, and unexpectedly, the expression level of CCL2 in BEAS-2B was higher than that in A549, which was contrary to expectations. Although the expression of CTSS in A549/Tax was significantly higher than in A549, the addition of tanshinone IIA did not significantly reduce its expression, and it was undetectable in BEAS-2B. Finally, only MMP7 was sequentially increased in BEAS-2B, A549, and A549/Tax, and its expression was significantly reduced in both A549 and A549/Tax after drug treatment. Further analysis using public data also indicated no significant difference in MMP2 expression between lung adenocarcinoma tissue and para-cancer tissue, while CCL2 and CTSS were significantly lower in lung adenocarcinoma tissue than in para-cancer tissue. MMP7 was higher in lung adenocarcinoma than in para-cancer tissue, which is consistent with the experimental results of this study. The results are shown in Fig. 2a–h. All N = 3.

3.3 Potential mechanism

In order to analyze the potential mechanism of tanshinone IIA inhibition on A549/Tax, we performed enrichment analysis of the MMP7 co-expression genes. We used the online tool GeneMANIA to obtain 21 co-expressed genes of MMP7 for subsequent enrichment analysis. The GO enrichment results indicated that processes such as extracellular matrix,

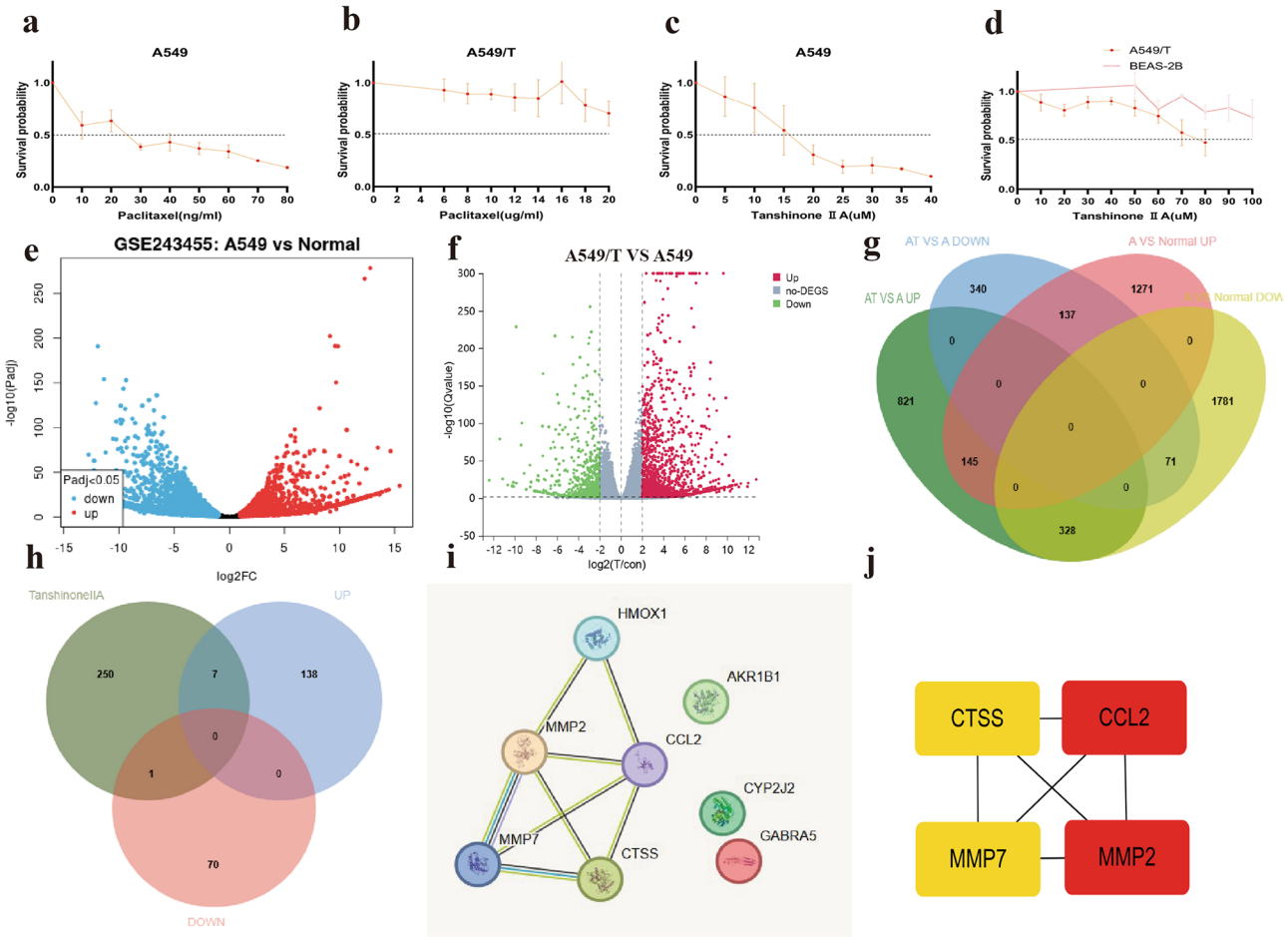

Fig. 1 Drug effectiveness and core target screening. **a** Paclitaxel is effective against A549; **b** A549/Tax showed significant resistance to paclitaxel; **c** Tanshinone IIA is effective against A549; **d** Tanshinone IIA is effective against A549/Tax and safe against BEAS-2B; **e** Differentially expressed genes between lung cancer and control; **f** Differentially expressed genes between A549/Tax and A549; **g** Genes that increase or decrease sequentially in healthy controls, A549, and A549/Tax; **h** The intersection gene of the stepped expression gene and the target of tanshinone IIA; **i** PPI networks of intersecting genes; **j** The underlying core genes

extracellular structure organization, and extracellular matrix disassembly were significantly enriched in BP, structures such as Golgi apparatus and lysosomes were significantly enriched in CC, and metalloendopeptidase, peptide chain endopeptidase, and metalloproteinase were significantly enriched in MF. Additionally, KEGG enrichment results showed that MMP7 co-expressed genes were significantly enriched in pathways such as ECM-receptor interaction and the PI3K-Akt signaling pathway. The results are shown in Fig. 3a–e.

3.4 Diagnostic and prognostic value of MMP7 in non-small cell lung cancer

To further analyze the potential value of MMP7 in non-small cell lung cancer, we analyzed the diagnostic and prognostic value of MMP7 in lung adenocarcinoma and lung squamous cell carcinoma. In the analysis of the diagnostic value of MMP7 for lung adenocarcinoma and squamous cell carcinoma, a total of 862 (including 288 healthy controls, 59 para-cancer data, and 515 cancer data) and 836 (including 288 healthy controls, 50 para-cancer data, and 498 cancer data) subjects were included. When analyzing the prognostic value of MMP7, a total of 598 lung adenocarcinoma data and 551 squamous cell carcinoma data were obtained. The ROC curve results indicated that the optimal cutoff values for MMP7 in diagnosing lung adenocarcinoma and squamous cell carcinoma were 4.2776 and 3.6656, respectively, with areas under the curve of 0.855 (0.830–0.879) and 0.863 (0.839–0.887), demonstrating good diagnostic performance. The Kaplan–Meier curves suggested that high expression of MMP7 may be a potential prognostic risk factor for lung

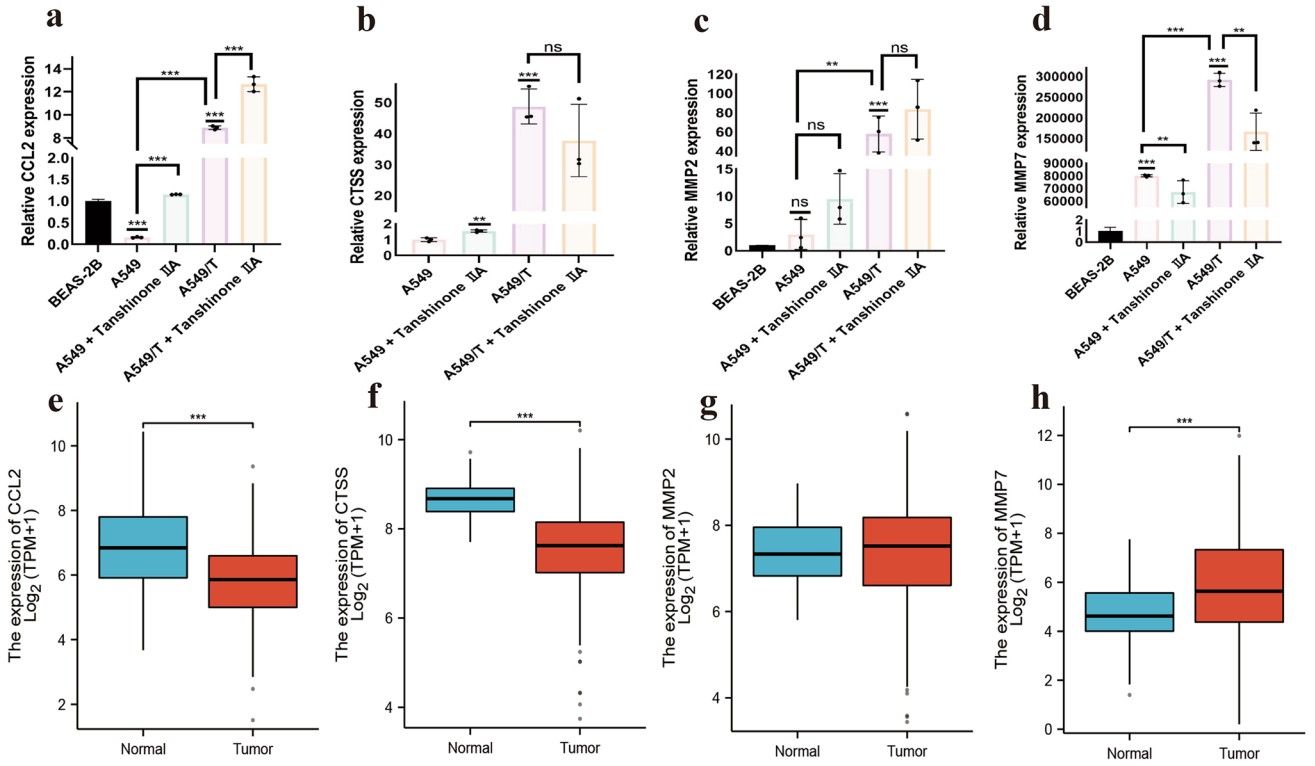

Fig. 2 Analysis (qPCR) and validation (TCGA) of potential core genes. **a** Compared with A549, the expression of CCL2 in A549/Tax was increased, and tanshinone IIA increased the expression of CCL2 in A549 and A549/Tax; **b** Compared with A549, the expression of CTSS in A549/Tax was increased, but tanshinone IIA did not decrease the expression of CTSS in A549/Tax; **c** Compared with A549, the expression of MMP2 in A549/Tax was increased, but tanshinone IIA did not decrease the expression of MMP2 in A549/Tax; **d** Compared with A549, the expression of MMP7 in A549/Tax is increased, and tanshinone IIA can reduce the expression of MMP7 in A549 and A549/Tax; **e** CCL2 expression decreased in lung cancer tissues compared with normal controls; **f** CTSS expression decreased in lung cancer tissues compared with normal controls; **g** There was no significant difference in the expression of MMP2 between the control group and lung cancer; **h** MMP7 expression was elevated in lung cancer compared to controls

adenocarcinoma (HR = 1.43, 95%CI: 1.07–1.91, P = 0.017) and squamous cell carcinoma (HR = 1.40, 95%CI: 1.06–1.85, P = 0.017). The results are shown in Fig. 3f–i.

3.5 Tanshinone IIA has good binding ability with PI3K, AKT, mTOR and MMP7

In order to preliminarily analyze the potential mechanism of tanshinone IIA inhibiting A549/Tax, we used molecular docking to analyze the docking potential of tanshinone IIA with PI3K, AKT, mTOR and MMP7. Molecular docking results showed that proteins PIK3R1, AKT1, mTOR, and MMP7 all exhibited high affinity with tanshinone IIA, with binding energies of − 8.1, − 12.3, − 9.3, and − 8.8 kcal/mol, respectively, indicating that the proteins have strong activity with the small molecule receptor and can bind under natural conditions. In addition, tanshinone IIA formed 2 hydrogen bonds with amino acid residue SER-460 in PIK3R1 protein, 1 hydrogen bond with amino acid residue SER-205 in AKT1 protein, 1 hydrogen bond with amino acid residue LYS-43 in mTOR protein, and 2 hydrogen bonds with amino acid residues ALA-210 and TYR-190 in MMP7 protein. At the same time, the four proteins made non-bonded contacts with tanshinone IIA, forming forces represented by electrostatic potential energy and van der Waals forces. The results are shown in Fig. 4a–d.

In order to further verify the reliability of the results of molecular docking, we carried out molecular dynamics simulation. The results showed that the RMSD values of PIK3R1, AKT1, mTOR and MMP7 fluctuated between 0.1–0.3 nm, 0.2–0.6 nm, 0.3–0.5 nm and 0.2–0.55 nm, respectively, during the whole simulation process, and all stabilized at the end, indicating their binding stability. The reason for the large RMSD value of the ligand corresponding to PIK3R1 may be that the large space of the binding site makes the ligand move in this region, but it converges and does not run out of the site at last. The results are shown in Supplementary Fig. 1a-d.

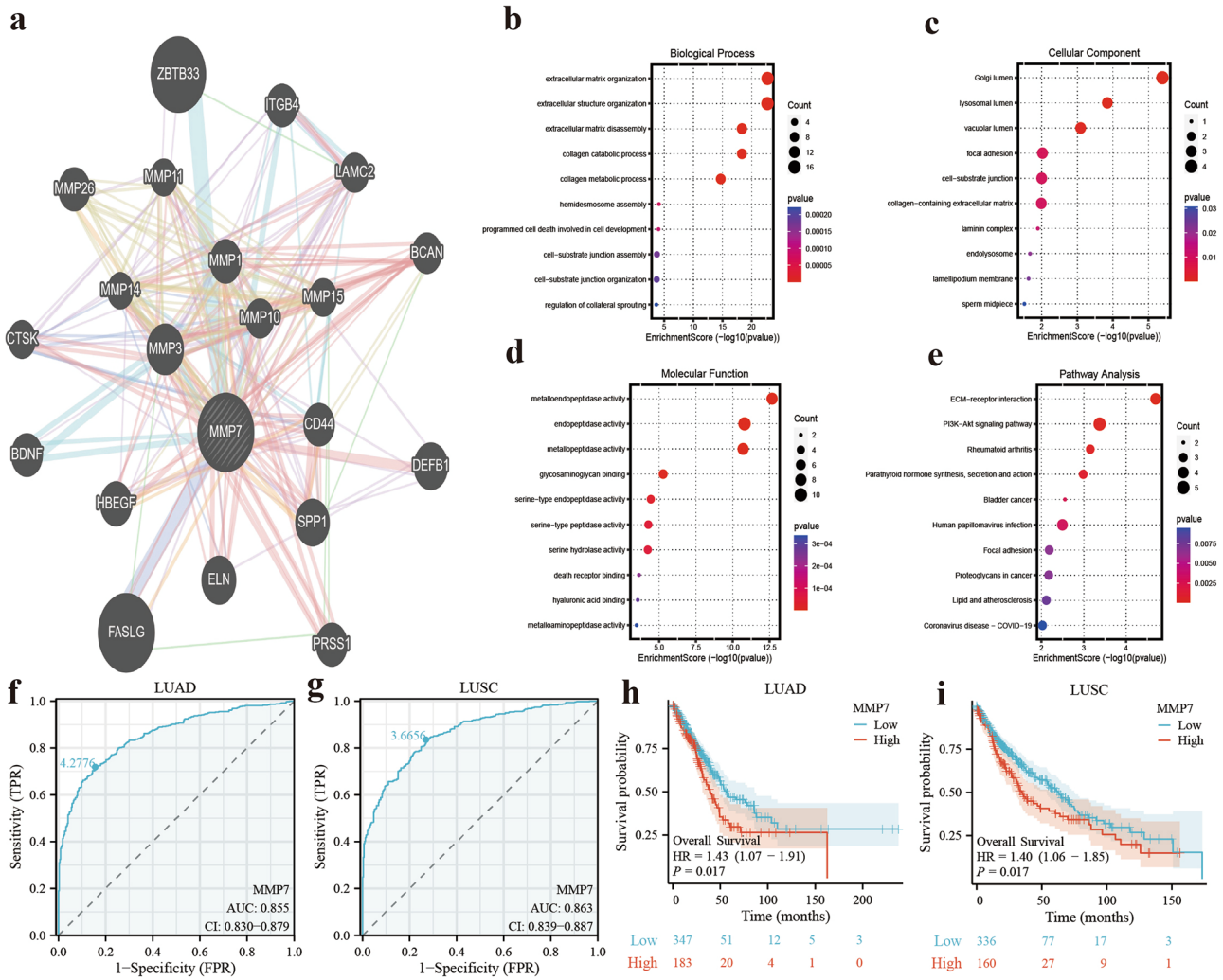

Fig. 3 Potential mechanisms of MMP7 and the value in the diagnosis and prognosis. **a** Co-expressed gene of MMP7; **b** Biological process enrichment results of co-expressed genes; **c** Cellular component enrichment results of co-expressed genes; **d** Molecular function enrichment results of co-expressed genes; **e** The results of KEGG enrichment of co-expressed genes suggest that the PI3K-AKT signaling pathway may play a key role; **f** Diagnostic value of MMP7 in lung adenocarcinoma; **g** Diagnostic value of MMP7 in lung squamous cell carcinoma; **h** The role of MMP7 in the prognosis of lung adenocarcinoma; **i** The role of MMP7 in the prognosis of lung squamous cell carcinoma

3.6 Tanshinone IIA affects the PI3K-AKT signaling pathway

To further verify the results of enrichment analysis and molecular docking, we analyzed the potential mechanism of tanshinone IIA inhibition of A549/Tax using western blot. Although our previous results showed that the IC50 of tanshinone IIA for A549 and A549/Tax is 15–20 and 70–80 μmol /L, respectively, these concentrations are too high during protein extraction and the 24-h survival rate of cells is too low. Therefore, in our follow-up experiments, the concentrations of tanshinone IIA applied to A549 and A549/Tax were 12 and 60 μmol /L, respectively. Western blotting results showed that after treatment with tanshinone IIA, the expression levels of BAX and BCL-2 both decreased, but the ratio of BAX to BCL-2 was not significantly different from that of the control group, indicating that the effect of tanshinone IIA on A549/Tax does not seem to be mediated through apoptosis. The results are shown in Supplementary Fig. 2a-b. Tanshinone IIA and BKM120 significantly reduced the expression of PI3K, p-AKT, AKT, mTOR, and MMP7 in A549/Tax, and this reduction could be blocked by 740 Y-P. Marimastat significantly reduced the expression of mTOR and MMP7 in A549/Tax, but did not affect PI3K, p-AKT, and AKT. The results of Western blotting again confirmed that the expression of MMP7 increased sequentially in BEAS-2B, A549, and A549/Tax, with significant differences. The above results suggest that marimastat affects the expression of MMP7 but not the PI3K-AKT signaling

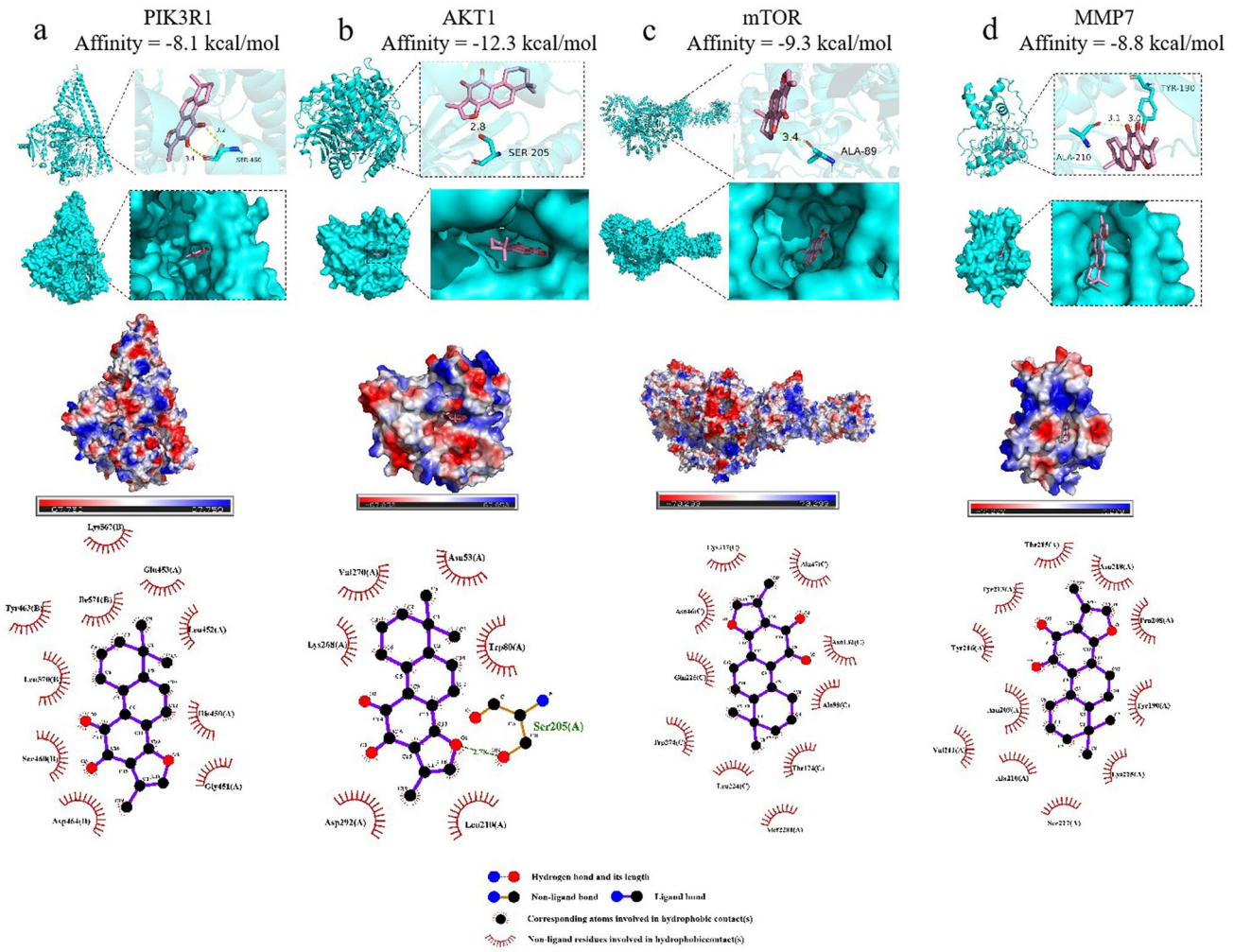

Fig. 4 Results of molecular docking. **a** Tanshinone IIA has good docking activity with PIK3R1; **b** Tanshinone IIA has good docking activity with AKT1; **c** Tanshinone IIA has good docking activity with mTOR; **d** Tanshinone IIA has good docking activity with MMP7

pathway, indicating that MMP7 is likely downstream of the PI3K-AKT pathway, and tanshinone IIA may inhibit the growth of A549/Tax by affecting the expression of MMP7 through the PI3K-AKT signaling pathway. The results are shown in Fig. 5a–f. All N = 3.

3.7 Potential value of marimastat and the combined effect of tanshinone IIA and paclitaxel

To further analyze whether marimastat, an inhibitor of MMP7, contributes to the inhibition of A549/Tax and whether marimastat has a combined effect with paclitaxel, we analyzed the inhibitory effects at different concentration combinations. The drug concentrations for each group were set as follows: Marimastat (100, 90, 80, 70, 60, 50, 0 μM), sensitivity restoration (Tanshinone IIA: 2 uM, paclitaxel: 30, 25, 20, 15, 10, 5, 0 μg/ml), combined effect (Tanshinone IIA: 50, 45, 40, 35, 30, 25, 0 μM, paclitaxel: 15, 12.5, 10, 7.5, 5, 2.5, 0 μM). CCK8 results indicated that marimastat has potential inhibitory effects on A549/Tax, but the IC50 was significantly greater than 100 μM, and marimastat showed no significant cytotoxic effect on BEAS-2B at concentrations between 50 and 100 μM. When exploring whether the combination of tanshinone IIA and paclitaxel could enhance the inhibitory effect on A549/Tax and whether tanshinone IIA could restore the sensitivity of A549/Tax to paclitaxel, the results showed that the combination of the two drugs did not significantly enhance the inhibitory effect on A549/Tax, and BEAS-2B was significantly inhibited within the experimental concentration range, which may be mainly due to the high concentration of paclitaxel or other unknown reactions between the drugs. The results are shown in Supplementary Fig. 2c-e. All N = 3.

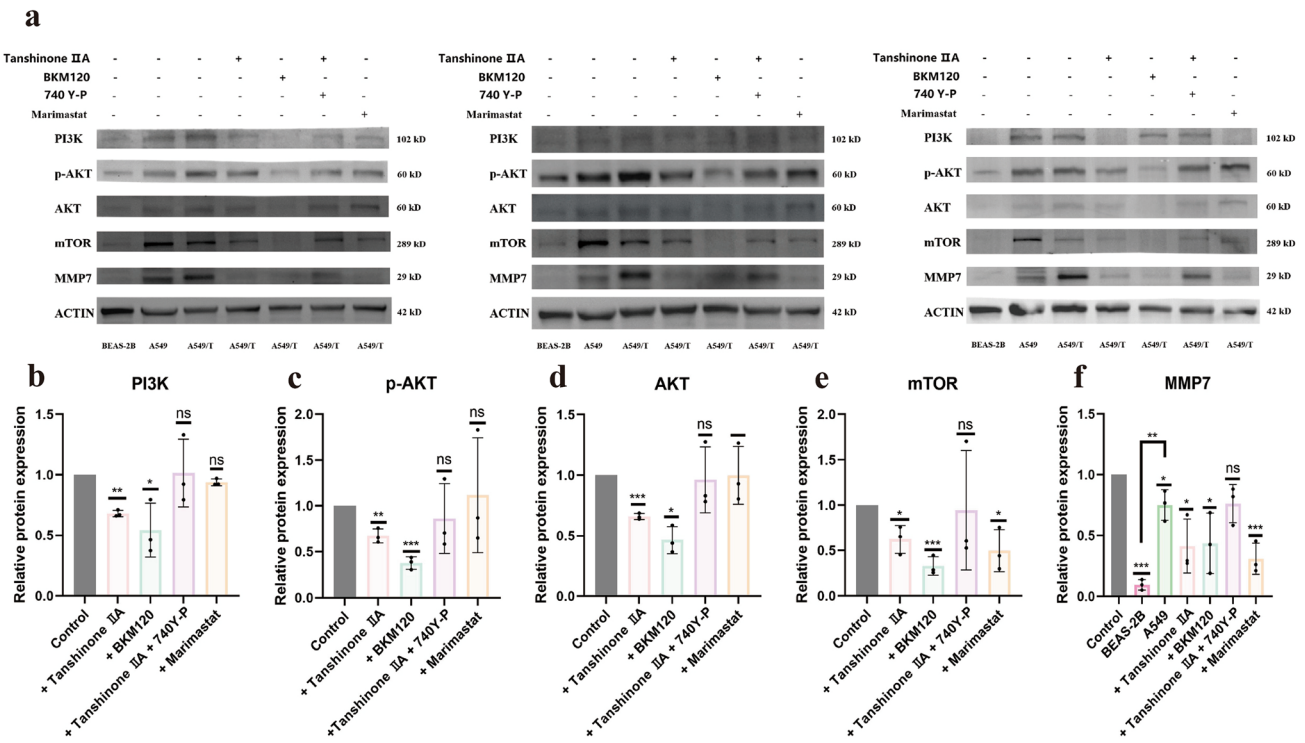

Fig. 5 Tanshinone IIA may act on A549/Tax through the PI3K-AKT signaling pathway. **a** Summary results of western blotting with three repeats; **b** Compared with the control group(A549/Tax), Tanshinone IIA and BKM120 decreased the expression of PI3K, 740Y-P could block the effect of tanshinone IIA, but Marimastat had no significant effect on the expression of PI3K; **c** Compared with the control group(A549/Tax), Tanshinone IIA and BKM120 decreased the expression of p-AKT, 740Y-P could block the effect of tanshinone IIA, but Marimastat had no significant effect on the expression of p-AKT; **d** Compared with the control group(A549/Tax), Tanshinone IIA and BKM120 decreased the expression of AKT, 740Y-P could block the effect of tanshinone IIA, but Marimastat had no significant effect on the expression of AKT; **e** Compared with the control group(A549/Tax), Tanshinone IIA, Marimastat and BKM120 decreased the expression of mTOR, 740Y-P could block the effect of tanshinone IIA; **f** The expression of MMP7 increased gradually in BEAS-2B, A549 and A549/Tax, Compared with the control group(A549/Tax), Tanshinone IIA, Marimastat and BKM120 decreased the expression of MMP7, 740Y-P could block the effect of tanshinone IIA

4 Discussion

This study initially used the CCK8 assay to preliminarily assess the inhibitory effect of tanshinone IIA on A549/Tax, then utilized transcriptome sequencing and publicly available data from GEO to explore RNA that shows stepwise changes in normal alveolar epithelium, non-small cell lung cancer, and paclitaxel-resistant non-small cell lung cancer. Potential core genes were further identified using drug action targets, and their accuracy was analyzed using qPCR and single-gene lung cancer analysis, with results indicating that only MMP7 met the predetermined conditions. Subsequent enrichment analysis of MMP7 co-expressed genes showed significant enrichment in the PI3K-AKT signaling pathway.

Previous studies have indicated that A549 cells may affect the expression of MMP7 through the PI3K/Akt signaling pathway, leading to paclitaxel resistance [37]. Multiple studies have shown that PI3K-AKT is related to drug resistance in lung cancer [38–41], and PI3K-AKT may affect the expression of MMP7 [42–44]. Additionally, MMP7 is associated with drug resistance in various cancers, including lung cancer [45–48]. Several studies have shown that tanshinone IIA is effective against resistance to osimertinib and gefitinib, and its inhibitory effect on various cancers, including lung cancer, may be exerted by affecting the PI3K-AKT signaling pathway [16, 49–51]. Therefore, it is particularly important to further analyze whether MMP7 plays a key role in the development of paclitaxel resistance in NSCLC and whether its expression is affected by the PI3K-AKT signaling pathway.

MMPs are a family of zinc-containing proteolytic enzymes that can promote tumor invasion, establishment of metastasis, and promotion of tumor-related angiogenesis [52]. Marimastat is an orally bioavailable matrix metalloproteinase inhibitor [53]. However, two previous clinical studies suggested that it may not improve the survival rate of lung cancer patients and could even have a negative impact on patients' quality of life [54, 55]. In recent years,

studies have also indicated that marimastat may be used to inhibit tumor metastasis and angiogenesis [56, 57]. The results of this study show that MMP7 increases sequentially in BEAS-2B, A549, and A549/Tax, and CCK8 results also suggest that marimastat may be effective against A549/Tax, but this requires more detailed research for analysis.

The results of this study indicate that tanshinone IIA may inhibit the expression of MMP7 by suppressing the PI3K-AKT-mTOR signaling pathway, thereby exerting its inhibitory effect on paclitaxel-resistant non-small cell lung cancer. Additionally, our research results suggest that tanshinone IIA affects tumor cell proliferation rather than apoptosis, which is consistent with previous studies on the inhibition of small cell lung cancer by tanshinone IIA [16]. Despite certain progress, there are still some unresolved issues in our study and the field as a whole, such as adverse drug reactions [58].

Although this study shows that tanshinone IIA is effective against A549/Tax and connects the PI3K-AKT signaling pathway with MMP7, there are still the following limitations: 1. This study partially relied on public datasets when screening core genes, but the dataset had results that did not match reality, preventing the discovery of more potential targets; 2. This study only explored the safety of tanshinone IIA on normal alveolar epithelial cells and did not analyze whether it would have adverse effects on the liver and kidneys; 3. The study results suggest that marimastat may also help inhibit the proliferation of A549/Tax, but this study did not conduct in-depth research; 4. Even though in vitro cell experiments demonstrated the effectiveness of tanshinone IIA, this study did not perform in vivo experiments for further validation; 5. Although we attempted to overexpress MMP7 in A549/Tax using a lentivirus (GOSL0196026, Shanghai Genechem Co., Ltd), the western blot results showed that the expression of MMP7 in A549/Tax after lentiviral transfection was lower compared to A549/Tax, as shown in Supplementary Fig. 2f-g.

5 Conclusions

Tanshinone IIA may affect the proliferation rather than apoptosis of A549/Tax by influencing the expression of MMP7 through the PI3K-AKT-mTOR signaling pathway, thereby exerting an anti-tumor effect.

Acknowledgements Not applicable.

Author contributions Conceptualization: C.F; Methodology: C.F; Software: C.F; Data curation: C.F and X.W; Investigation: C.F and X.W; Validation: C.F; Formal analysis: C.F and X.W; Supervision: Q.G; Funding acquisition: Q.G; Visualization: C.F; Project administration: Q.G; Resources: Q.G; Writing—original draft: C.F; Writing—review & editing: all authors.

Funding This study was supported by the Clinical Key Project of Peking University Third Hospital (BYSYRCYJ2023001).

Data availability Data available in article supplementary material.

Declarations

Ethics approval and consent to participate Not applicable.

Consent for publication Not applicable.

Competing interests The authors declare no competing interests.

References

1. Sands J, Tammemägi MC, Couraud S, Baldwin DR, Borondy-Kitts A, Yankelevitz D, Lewis J, Grannis F, Kauczor HU, von Stackelberg O, et al. Lung screening benefits and challenges: a review of the data and outline for implementation. J Thorac Oncol. 2021;16(1):37–53.
2. Siegel RL, Miller KD, Jemal A. Cancer statistics, 2020. CA Cancer J Clin. 2020;70(1):7–30.

3. Remon J, Soria JC, Peters S. Early and locally advanced non-small-cell lung cancer: an update of the ESMO clinical practice guidelines focusing on diagnosis, staging, systemic and local therapy. Ann Oncol. 2021;32(12):1637–42.
4. Relli V, Trerotola M, Guerra E, Alberti S. Abandoning the notion of non-small cell lung cancer. Trends Mol Med. 2019;25(7):585–94.
5. Siegel RL, Miller KD, Fuchs HE, Jemal A. Cancer statistics, 2021. CA Cancer J Clin. 2021;71(1):7–33.
6. Bai Y, Xiong L, Zhu M, Yang Z, Zhao J, Tang H. Co-expression network analysis identified KIF2C in association with progression and prognosis in lung adenocarcinoma. Cancer Biomark. 2019;24(3):371–82.
7. Zappa C, Mousa SA. Non-small cell lung cancer: current treatment and future advances. Transl Lung Cancer Res. 2016;5(3):288–300.
8. Li MY, Liu LZ, Dong M. Progress on pivotal role and application of exosome in lung cancer carcinogenesis, diagnosis, therapy and prognosis. Mol Cancer. 2021;20(1):22.
9. Yang Y, Qian Z, Feng M, Liao W, Wu Q, Wen F, Li Q. Study on the prognosis, immune and drug resistance of m6A-related genes in lung cancer. BMC Bioinform. 2022;23(1):437.
10. Doroshow DB, Sanmamed MF, Hastings K, Politi K, Rimm DL, Chen L, Melero I, Schalper KA, Herbst RS. Immunotherapy in non-small cell lung cancer: facts and hopes. Clin Cancer Res. 2019;25(15):4592–602.
11. Cowper PA, Feng L, Kosinski AS, Tong BC, Habib RH, Putnam JB Jr, Onaitis MW, Furnary AP, Wright CD, Jacobs JP, et al. Initial and longitudinal cost of surgical resection for lung cancer. Ann Thorac Surg. 2021;111(6):1827–33.
12. Imyanitov EN, Iyevleva AG, Levchenko EV. Molecular testing and targeted therapy for non-small cell lung cancer: current status and perspectives. Crit Rev Oncol Hematol. 2021;157:103194.
13. Mohammad-Jafari K, Naghib SM, Mozafari MR. Liposomal nanoformulation-encapsulated paclitaxel for reducing chemotherapy side effects in lung cancer treatments: recent advances and future outlooks. Curr Med Chem. 2024. https://doi.org/10.2174/0109298673308951240921121345.
14. Zhang R, Chen P, Wang Y, Zeng Z, Yang H, Li M, Liu X, Yu W, Hou P. Targeting METTL3 enhances the chemosensitivity of non-small cell lung cancer cells by decreasing ABCC2 expression in an m(6)A-YTHDF1-dependent manner. Int J Biol Sci. 2024;20(12):4750–66.
15. Meyer ML, Fitzgerald BG, Paz-Ares L, Cappuzzo F, Jänne PA, Peters S, Hirsch FR. New promises and challenges in the treatment of advanced non-small-cell lung cancer. Lancet. 2024;404(10454):803–22.
16. Jiang Y, Bi Y, Zhou L, Zheng S, Jian T, Chen J. Tanshinone IIA inhibits proliferation and migration by downregulation of the PI3K/Akt pathway in small cell lung cancer cells. BMC Complement Med Ther. 2024;24(1):68.
17. Xu H, Guo NN, Zhu CY, Ye LY, Yan XY, Liu YQ, Zhang ZY, Zhang G, Hussain L. Diterpenoid tanshinones can inhibit lung cancer progression by improving the tumor microenvironment and downregulation of NF-κB expression. ACS Omega. 2024;9(6):7230–8.
18. Sun F, Yang X, Song W, Yu N, Lin Q. Tanshinone IIA (TSIIA) represses the progression of non-small cell lung cancer by the circ_0020123/miR-1299/HMGB3 pathway. Mol Cell Biochem. 2023;478(9):1973–86.
19. Cao L, Qin Z, Yu T, Bai X, Jiang S, Wang D, Ning F, Huang M, Jin J. Tanshinone IIA acts as a regulator of lipogenesis to overcome osimertinib acquired resistance in lung cancer. Biochem Pharmacol. 2024;224:116207.
20. Wang R, Luo Z, Zhang H, Wang T. Tanshinone IIA reverses Gefitinib-resistance in human non-small-cell lung cancer via regulation of VEGFR/Akt pathway. Onco Targets Ther. 2019;12:9355–65.
21. Zhang L, Xu C, Huang J, Jiang S, Qin Z, Cao L, Tan G, Zhao Z, Huang M, Jin J. Tanshinone IIA reverses gefitinib resistance in EGFR-mutant lung cancer via inhibition of SREBP1-mediated lipogenesis. Phytother Res. 2024;38(3):1574–88.
22. Zhang YZ, Lai HL, Huang C, Jiang ZB, Yan HX, Wang XR, Xie C, Huang JM, Ren WK, Li JX, et al. Tanshinone IIA induces ER stress and JNK activation to inhibit tumor growth and enhance anti-PD-1 immunotherapy in non-small cell lung cancer. Phytomedicine. 2024;128:155431.
23. Liao XZ, Gao Y, Huang S, Chen ZZ, Sun LL, Liu JH, Chen HR, Yu L, Zhang JX, Lin LZ. Tanshinone IIA combined with cisplatin synergistically inhibits non-small-cell lung cancer in vitro and in vivo via down-regulating the phosphatidylinositol 3-kinase/Akt signalling pathway. Phytother Res. 2019;33(9):2298–309.
24. Xie J, Liu JH, Liu H, Liao XZ, Chen Y, Lin MG, Gu YY, Liu TL, Wang DM, Ge H, et al. Tanshinone IIA combined with adriamycin inhibited malignant biological behaviors of NSCLC A549 cell line in a synergistic way. BMC Cancer. 2016;16(1):899.
25. Franz M, Rodriguez H, Lopes C, Zuberi K, Montojo J, Bader GD, Morris Q. GeneMANIA update 2018. Nucleic Acids Res. 2018;46(W1):W60-w64.
26. Vivian J, Rao AA, Nothaft FA, Ketchum C, Armstrong J, Novak A, Pfeil J, Narkizian J, Deran AD, Musselman-Brown A, et al. Toil enables reproducible, open source, big biomedical data analyses. Nat Biotechnol. 2017;35(4):314–6.
27. Liu J, Lichtenberg T, Hoadley KA, Poisson LM, Lazar AJ, Cherniack AD, Kovatich AJ, Benz CC, Levine DA, Lee AV, et al. An integrated TCGA pan-cancer clinical data resource to drive high-quality survival outcome analytics. Cell. 2018;173(2):400-416.e411.
28. Seeliger D, de Groot BL. Ligand docking and binding site analysis with PyMOL and Autodock/Vina. J Comput Aided Mol Des. 2010;24(5):417–22.
29. Trott O, Olson AJ. AutoDock Vina: improving the speed and accuracy of docking with a new scoring function, efficient optimization, and multithreading. J Comput Chem. 2010;31(2):455–61.
30. de Vlieg J, Scheek RM, van Gunsteren WF, Berendsen HJ, Kaptein R, Thomason J. Combined procedure of distance geometry and restrained molecular dynamics techniques for protein structure determination from nuclear magnetic resonance data: application to the DNA binding domain of lac repressor from *Escherichia coli*. Proteins. 1988;3(4):209–18.
31. Essmann U, Berkowitz ML. Dynamical properties of phospholipid bilayers from computer simulation. Biophys J. 1999;76(4):2081–9.
32. Hess B. P-LINCS: a parallel linear constraint solver for molecular simulation. J Chem Theory Comput. 2008;4(1):116–22.
33. Zhou X, Li R, Chen R, Liu J. Altered mitochondrial dynamics, biogenesis, and functions in the paclitaxel-resistant lung adenocarcinoma cell line A549/Taxol. Med Sci Monit. 2020;26: e918216.
34. Han ML, Zhao YF, Tan CH, Xiong YJ, Wang WJ, Wu F, Fei Y, Wang L, Liang ZQ. Cathepsin L upregulation-induced EMT phenotype is associated with the acquisition of cisplatin or paclitaxel resistance in A549 cells. Acta Pharmacol Sin. 2016;37(12):1606–22.
35. Xie CQ, Zhou P, Zuo J, Li X, Chen Y, Chen JW. Triptolide exerts pro-apoptotic and cell cycle arrest activity on drug-resistant human lung cancer A549/Taxol cells via modulation of MAPK and PI3K/Akt signaling pathways. Oncol Lett. 2016;12(5):3586–90.
36. Li Z, Zhang Y, Zhou Y, Wang F, Yin C, Ding L, Zhang S. Tanshinone IIA suppresses the progression of lung adenocarcinoma through regulating CCNA2-CDK2 complex and AURKA/PLK1 pathway. Sci Rep. 2021;11(1):23681.

37. Keeratichamroen S, Lirdprapamongkol K, Svasti J. Mechanism of ECM-induced dormancy and chemoresistance in A549 human lung carcinoma cells. Oncol Rep. 2018;39(4):1765–74.
38. Di J, Bo W, Wang C, Liu C. Ailanthone increases cisplatin-induced apoptosis and autophagy in cisplatin resistance non-small cell lung cancer cells through the PI3K/AKT/mTOR pathway. Curr Med Chem. 2024. https://doi.org/10.2174/0109298673315460240816091032.
39. Huang W, Guo Y, Qian Y, Liu X, Li G, Wang J, Yang X, Wu M, Fan Y, Luo H, et al. Ferroptosis-inducing compounds synergize with docetaxel to overcome chemoresistance in docetaxel-resistant non-small cell lung cancer cells. Eur J Med Chem. 2024;276:116670.
40. Huang YH, Chiu LY, Tseng JS, Hsu KH, Chen CH, Sheu GT, Yang TY. Attenuation of PI3K-Akt-mTOR pathway to reduce cancer stemness on chemoresistant lung cancer cells by shikonin and synergy with BEZ235 inhibitor. Int J Mol Sci. 2024;25(1):616.
41. Li R, Zhao W, Jin C, Xiong H. Novel 4-Amino-Quinazoline moieties ligated Platinum(IV) prodrugs overcome cisplatin resistance in EGFR(WT) human lung cancer. Bioorg Chem. 2023;135:106499.
42. Lee J, Lim JW, Kim H. Astaxanthin inhibits matrix metalloproteinase expression by suppressing PI3K/AKT/mTOR activation in helicobacter pylori-infected gastric epithelial cells. Nutrients. 2022;14(16):3427.
43. Lu Y, Zhang Y, Pan Z, Yang C, Chen L, Wang Y, Xu D, Xia H, Wang S, Chen S, et al. Potential "therapeutic" effects of tocotrienol-rich fraction (TRF) and carotene "against" bleomycin-induced pulmonary fibrosis in rats via TGF-β/Smad, PI3K/Akt/mTOR and NF-κB signaling pathways. Nutrients. 2022;14(5):1094.
44. Dai B, Yu R, Fan M, Yang T, Wang B, Zhang Y. HMQ-T-F2 suppresses migration of the human cervical cancer HeLa cells by reversing EMT via the PI3K/Akt signaling pathway. Oncol Rep. 2019;42(4):1451–8.
45. Liao J, Chen Z, Yu Z, Huang T, Hu D, Su Y, He Z, Zou C, Zhang L, Lin X. The role of ARL4C in erlotinib resistance: activation of the Jak2/Stat 5/β-catenin signaling pathway. Front Oncol. 2020;10:585292.
46. Yu WH, Wu E, Li Y, Hou HH, Yu SC, Huang PT, Kuo WH, Qi D, Yu CJ. Matrix metalloprotease-7 mediates nucleolar assembly and intra-nucleolar cleaving p53 in Gefitinib-resistant cancer stem cells. iScience. 2020;23(10):101600.
47. Deng QF, Fang QY, Ji XX, Zhou SW. Cyclooxygenase-2 mediates gefitinib resistance in non-small cell lung cancer through the EGFR/PI3K/AKT axis. J Cancer. 2020;11(12):3667–74.
48. Ohashi S, Natsuizaka M, Nakagawa H. MMP7 and activation of IGF-1R: a new insight into anti-EGFR therapeutic resistance in metastatic colorectal cancer. Cancer Biol Ther. 2011;11(2):184–7.
49. Tang N, Wang Y, Miao J, Zhao Y, Cao Y, Sun W, Zhang J, Sui H, Li B. Potential pharmacological mechanisms of tanshinone IIA in the treatment of human neuroblastoma based on network pharmacological and molecular docking Technology. Front Pharmacol. 2024;15:1363415.
50. Qin C, Liu S, Zhou S, Xia X, Hu J, Yu Y, Ma D. Tanshinone IIA promotes vascular normalization and boosts Sorafenib's anti-hepatoma activity via modulating the PI3K-AKT pathway. Front Pharmacol. 2023;14:1189532.
51. Liu H, Liu C, Wang M, Sun D, Zhu P, Zhang P, Tan X, Shi G. Tanshinone IIA affects the malignant growth of Cholangiocarcinoma cells by inhibiting the PI3K-Akt-mTOR pathway. Sci Rep. 2021;11(1):19268.
52. Bonomi P. Matrix metalloproteinases and matrix metalloproteinase inhibitors in lung cancer. Semin Oncol. 2002;29(1 Suppl 4):78–86.
53. Goffin JR, Anderson IC, Supko JG, Eder JP Jr, Shapiro GI, Lynch TJ, Shipp M, Johnson BE, Skarin AT. Phase I trial of the matrix metalloproteinase inhibitor marimastat combined with carboplatin and paclitaxel in patients with advanced non-small cell lung cancer. Clin Cancer Res. 2005;11(9):3417–24.
54. Shepherd FA, Giaccone G, Seymour L, Debruyne C, Bezjak A, Hirsh V, Smylie M, Rubin S, Martins H, Lamont A, et al. Prospective, randomized, double-blind, placebo-controlled trial of marimastat after response to first-line chemotherapy in patients with small-cell lung cancer: a trial of the National cancer institute of Canada-clinical trials group and the European organization for research and treatment of cancer. J Clin Oncol. 2002;20(22):4434–9.
55. Coudert B. Marimastat may not improve survival over placebo following induction therapy for small-cell lung cancer. Cancer Treat Rev. 2003;29(2):127–9.
56. Lyu Y, Xiao Q, Yin L, Yang L, He W. Potent delivery of an MMP inhibitor to the tumor microenvironment with thermosensitive liposomes for the suppression of metastasis and angiogenesis. Signal Transduct Target Ther. 2019;4:26.
57. Lv Y, Zhao X, Zhu L, Li S, Xiao Q, He W, Yin L. Targeting intracellular MMPs efficiently inhibits tumor metastasis and angiogenesis. Theranostics. 2018;8(10):2830–45.
58. Yang C, Mu Y, Li S, Zhang Y, Liu X, Li J. Tanshinone IIA: a Chinese herbal ingredient for the treatment of atherosclerosis. Front Pharmacol. 2023;14:1321880.